Redox Potential Measurements of the *Mycobacterium tuberculosis* Heme Protein KatG and the Isoniazid-Resistant Enzyme KatG(S315T): Insights into Isoniazid Activation

Nancy L. Wengenack,[‡] Helder Lopes,[§] Matthew J. Kennedy,[‡,||] Pedro Tavares,[§] Alice S. Pereira,[§] Isabel Moura,[§] José J. G. Moura,[§] and Frank Rusnak*[,‡]

Department of Biochemistry and Molecular Biology and Section of Hematology Research, Mayo Clinic, Rochester, Minnesota 55905, and Departamento de Química, Centro de Química Fina e Biotecnologia, Faculdade de Ciências e Tecnologia, Universidade Nova de Lisboa, 2825-114 Caparica, Portugal

Received May 31, 2000

ABSTRACT: *Mycobacterium tuberculosis* KatG is a multifunctional heme enzyme responsible for activation of the antibiotic isoniazid. A KatG(S315T) point mutation is found in >50% of isoniazid-resistant clinical isolates. Since isoniazid activation is thought to involve an oxidation reaction, the redox potential of KatG was determined using cyclic voltammetry, square wave voltammetry, and spectroelectrochemical titrations. Isoniazid activation may proceed via a cytochrome P450-like mechanism. Therefore, the possibility that substrate binding by KatG leads to an increase in the heme redox potential and the possibility that KatG(S315T) confers isoniazid resistance by altering the redox potential were examined. Effects of the heme spin state on the reduction potentials of KatG and KatG(S315T) were also determined. Assessment of the Fe^{3+}/Fe^{2+} couple gave a midpoint potential of ca. −50 mV for both KatG and KatG(S315T). In contrast to cytochrome P450s, addition of substrate had no significant effect on either the KatG or KatG(S315T) redox potential. Conversion of the heme to a low-spin configuration resulted in a −150 to −200 mV shift of the KatG and KatG(S315T) redox potentials. These results suggest that isoniazid resistance conferred by KatG(S315T) is not mediated through changes in the heme redox potential. The redox potentials of isoniazid were also determined using cyclic and square wave voltammetry, and the results provide evidence that the ferric KatG and KatG(S315T) midpoint potentials are too low to promote isoniazid oxidation without formation of a high-valent enzyme intermediate such as compounds I and II or oxyferrous KatG.

One-third of the world's population is infected with *Mycobacterium tuberculosis*, and nearly 2 million deaths result from tuberculosis each year (*1*). Isoniazid, one of the most popular antibiotics used to treat TB,[1] is a prodrug activated by the mycobacterial enzyme KatG, a hemoprotein possessing catalase-peroxidase, Mn^{2+}-dependent peroxidase, cytochrome P450-like oxygenase, and peroxynitritase activities (*2*−*8*). Targets of activated isoniazid include InhA and KasA, enzymes involved in the synthesis of mycolic acids which are components of the mycobacterial cell wall (*9*, *10*). The identity of activated isoniazid is unknown, but details regarding the activation mechanism are beginning to emerge.

Isoniazid-resistant clinical isolates of *M. tuberculosis* often have a single-point mutation in KatG which converts a serine at amino acid residue 315 to a threonine [KatG(S315T)]. At present, a three-dimensional structure of KatG is not available, but on the basis of the similarity with *Saccharomyces cerevisiae* CCP, amino acid residue 315 (analogous to CCP serine 185) has been hypothesized to occupy a region approximately 11 Å from the heme iron, forming a hydrogen bond with a heme propionate (*11*). The S315T mutation is found in >50% of resistant isolates and confers at least a 10-fold increase in the minimal inhibitory concentration for isoniazid in vivo (*11*−*16*).

We have recently shown that neither the catalase-peroxidase nor the Mn^{2+}-dependent peroxidase activity of KatG correlates with isoniazid susceptibility (*6*, *17*). Others have proposed that oxyferrous KatG (Fe^{2+}−OO) can act as an oxidant of isoniazid through a mechanism analogous to that used by the cytochrome P450 family of enzymes (*7*). Substrate binding by cytochrome P450s often causes the heme to undergo conversion from a six-coordinate low-spin to a five-coordinate high-spin configuration (*18*). The spin transition results in a significant increase in the redox potential of the ferric iron, thus facilitating electron transfer to yield the reduced (Fe^{2+}) enzyme (*19*). Upon reduction, oxygen binds to the ferrous iron forming an oxyferrous intermediate, the precursor to the high-valent species thought to be responsible for substrate oxidation. In an analogous

* To whom correspondence should be addressed: Section of Hematology Research, Department of Biochemistry and Molecular Biology, Mayo Clinic, 200 First Street, SW, Rochester, MN 55905. Telephone: (507) 284-4743. Fax: (507) 284-8286. E-mail: rusnak@mayo.edu.

‡ Mayo Clinic.

§ Universidade Nova de Lisboa.

|| Current address: Department of Biochemistry, University of Washington, Seattle, WA 98105.

[1] Abbreviations: CCP, cytochrome *c* peroxidase; CN, cyanide; CV, cyclic voltammetry; *E*°, reduction potential; E_p, pulse potential; INH, isoniazid; i_p, net peak current; NHE, normal hydrogen electrode; SWV, square wave voltammetry; TB, tuberculosis.

10.1021/bi001239v CCC: $19.00
Published on Web 08/23/2000

fashion, isoniazid binding to KatG results in an increase in the proportion of five-coordinate high-spin heme (*20*). KatG(S315T) binds isoniazid near the heme periphery at a distance indistinguishable from its position in the wild-type enzyme. However, the KatG(S315T) heme does not undergo a spin transition upon isoniazid binding and experiences a 3−6-fold reduction in the rate of isoniazid oxidation (*6*, *17*, *20*, *21*). We have reported that oxyferrous KatG can be formed by binding of superoxide to the ferric heme and demonstrated that KatG(S315T) displays an at least 10-fold reduction in reactivity toward superoxide relative to the wild-type enzyme (*17*). Together, these results led us to determine whether isoniazid binding is accompanied by an increase in the midpoint potential of the KatG Fe^{3+}/Fe^{2+} couple. Further, the possibility that the S315T mutation may change the reactivity of the heme iron possibly through alteration of the heme redox potential was examined.

An understanding of the KatG reduction potential is a fundamental requirement for elucidation of the precise mechanism of isoniazid activation. In this work, we utilize cyclic and square wave voltammetry together with spectroelectrochemical titrations to determine for the first time the reduction potential of *M. tuberculosis* KatG. In addition, the effect of the KatG(S315T) mutation, isoniazid binding, and heme spin state on the enzyme reduction potential was determined. Reduction potentials for isoniazid were also determined using cyclic and square wave voltammetry. Comparison of the ferric KatG reduction potential with that required for isoniazid oxidation suggests a mechanism for the KatG-dependent, one-electron oxidation of isoniazid to a hydrazyl radical by either KatG compounds I and II or oxyferrous KatG.

MATERIALS AND METHODS

Protein Preparation. The expression and purification of recombinant *M. tuberculosis* KatG and KatG(S315T) in *Escherichia coli* have been described previously (*6*). The protein concentration was determined using Pierce (Rockford, IL) Coomassie plus Protein reagent with bovine serum albumin as the standard (*22*). The A_{408}/A_{280} ratio, a spectroscopic measure of hemoprotein purity, was 0.65 and 0.64 for KatG and KatG(S315T), respectively, indicating that both enzymes were purified to near homogeneity (*23*).

Cyclic and Square Wave Voltammetry. Cyclic and square wave voltammograms were obtained using a Princeton Applied Research (Oak Ridge, TN) model 273 potentiostat. Automated data acquisition was achieved by data transfer to a Zenith PC/AT desktop computer via a GPIB-PC2 interface (National Instruments, Austin, TX). A graphite working electrode was polished with aluminum oxide (particle size of 0.075 μm), and excess particles were removed by electrode sonication in a water bath for 5 min prior to each use. The counter electrode was a platinum wire, and the reference was a saturated Ag/AgCl electrode. A two-compartment electrochemical cell separated by porous glass was filled with 100 μL of sample solution. Oxygen was removed by passing H_2O-saturated argon gas over solutions for 15 min prior to use. The cell was also purged of oxygen using argon prior to sample addition, and an anaerobic atmosphere was maintained throughout the analysis. Solutions contained 200 μM KatG or KatG(S315T), 100 mM KCl (supporting electrolyte), and 2 mM neomycin (a promoter which improves interaction of the enzyme with the electrode surface) in 50 mM sodium phosphate buffer (pH 7.6). Where appropriate, 400 μM isoniazid or 200 μM sodium cyanide was added to the solution.

Cyclic voltammetry utilizes a triangular waveform applied between two potentials in both the forward and reverse directions, with the current measured at the working electrode during the potential scan (*24*). For a reversible redox couple, $E°$ is centered between the anodic and cathodic peak potentials (*24*). Square wave voltammetry is conducted by varying the potential versus time in the form of a staircase waveform (*25*). Relevant parameters include the anodic and cathodic E_p and the time between the applied steps (τ). The inverse of τ is the frequency of the step potential. The resulting current is measured at the completion of each pulse, and the difference between the anodic and cathodic current is calculated. The net peak current, i_p, is centered on the reversible equilibrium potential. In this work, $E_p = 25$ mV and $\tau^{-1} = 8$ Hz. Compared with other techniques such as polarography and cyclic voltammetry, square wave voltammetry offers the advantage of greater analysis speed. As a result, problems with electrode fouling are reduced, making this an attractive technique for protein analysis. The increased speed also means square wave voltammetry can detect reversible reactions not observed using slower techniques that can suffer due to unwanted chemical side reactions.

Spectroelectrochemistry. The midpoint reduction potentials of KatG and KatG(S315T) were also determined by spectroelectrochemical titration using a cell adapted from that of Stankovich (*26*). Reductive and oxidative titrations were conducted in a stirred, anaerobic cuvette constantly flushed with H_2O-saturated argon. The potential was measured at a gold working electrode referenced to an Ag/AgCl electrode. Analyte solutions contained 9 μM KatG or KatG(S315T) in 50 mM sodium phosphate buffer (pH 7.6). Mediators used to promote electron transfer between the protein and the working electrode included 1,2-naphthoquinone (180 mV versus NHE), phenazine methosulfate (80 mV), 1,4-naphthoquinone (60 mV), 5-hydroxy-1,4-naphthoquinone (30 mV), duroquinone (5 mV), methylene blue (11 mV), indigo tetrasulfonate (−46 mV), phenazine (−125 mV), and 2-hydroxy-1,4-naphthoquinone (−145 mV). The concentration of each mediator was 0.09 μM, giving a 1:100 ratio of mediator to protein. Reductive titrations were carried out by sequential additions of 50 mM sodium dithionite (pH 8.0), while oxidative titrations were conducted using potassium ferricyanide as the titrant. The spectrum was recorded and the potential measured following attainment of equilibrium after each addition of titrant. Equilibrium was defined as a potential change of <1 mV/min. Spectra were recorded using a Cary model 1 dual-beam spectrophotometer, and the sample temperature was maintained at 25 °C. The reduction potential was determined by fitting the titration progress curve (normalized absorbance vs potential) to the Nernst equation (using MacCurve Fit version 1.3.5, Kevin Raner Software, Mt. Waverley, Victoria, Australia):

$$E = E° - \frac{2.3RT}{nF}\log\frac{[\text{oxidized}]}{[\text{reduced}]} \qquad (1)$$

where R is the gas constant, F is Faraday's constant, T is

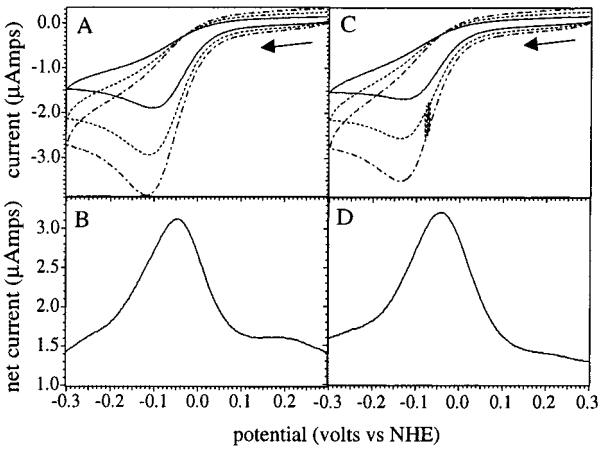

FIGURE 1: Voltammograms of KatG and KatG(S315T). Solutions contained 200 μM KatG or KatG(S315T) in 100 mM sodium phosphate buffer (pH 7.6) with 100 mM KCl and 2 mM neomycin, and voltammograms were recorded using a graphite electrode: (A) cyclic voltammogram of KatG at 20 (solid line), 50 (dashed line), and 80 mV/s (dashed−dotted line), (B) square wave voltammogram of KatG ($E_p = 25$ mV and $\tau^{-1} = 8$ Hz), (C) cyclic voltammogram of KatG(S315T) at 20 (solid line), 50 (dashed line), and 80 mV/s (dashed−dotted line), and (D) square wave voltammogram of KatG(S315T) ($E_p = 25$ mV and $\tau^{-1} = 8$ Hz).

the temperature (kelvin), and n is the number of electrons transferred per mole of analyte.

Reduction Potentials. Throughout this paper, reduction potentials are reported with reference to the NHE and were obtained by adding 199 mV to E_{obs} versus the Ag/AgCl electrode (*27*). All reported potentials are the means ± the standard deviation of at least three measurements unless otherwise noted.

RESULTS

KatG and KatG(S315T) Reduction Potentials. The cyclic and square wave voltammograms for KatG and KatG(S315T) at 25 °C in 50 mM sodium phosphate buffer (pH 7.6) are shown in Figure 1. Upon reduction, the cyclic voltammograms for KatG and KatG(S315T) each display a cathodic peak with a maximum at ca. −0.12 V versus the NHE, which is not reversible even at high scan rates (Figure 1A,C). Increasing the scan rate up to 1 V/s did not affect the reversibility of the waveform (Figure 1A,C and data not shown). This type of behavior is characteristic of an electrochemically irreversible system where a fast electron transfer step is followed by an irreversible chemical reaction, resulting in the loss of the return peak at each transition potential (*28*). Examples of such reactions might include interaction with solvent or diffusion of the product from the electrode surface. It is possible to estimate $E°$ from the cyclic voltammograms by assuming a one-electron process at each transition. The forward and reverse waves should then be separated by 59 mV, and $E°$ is centered between the peaks of the two waves (*24*). Using this assumption, $E°$ was estimated to be ca. −80 mV for KatG and ca. −100 mV for KatG(S315T).

SWV was used in an attempt to circumvent side reactions and allowed direct determination of $E°$. Using SWV, KatG exhibits a symmetrical peak with an $E°$ of ca. −50 mV (Figure 1B), while KatG(S315T) also exhibits a peak centered at ca. −50 mV (Figure 1D) versus the NHE. A summary of reduction potentials determined from repeated trials is presented in Table 1.

Table 1: Redox Potentials[a] of KatG and KatG(S315T)

	technique	$E°$ (mV vs NHE)
KatG	SWV	−58 ± 24
KatG	spectroelectrochemical titration	−28 ± 17
KatG(S315T)	SWV	−77 ± 35
KatG(S315T)	spectroelectrochemical titration	−21 ± 18
KatG + INH	SWV	−45 ± 27
KatG(S315T) + INH	SWV	−67 ± 27
KatG + CN	SWV	−197 ± 19
KatG(S315T) + CN	SWV	−251[b]

[a] All values are the means ± the standard deviation of three experiments unless otherwise noted. [b] Average of two experiments.

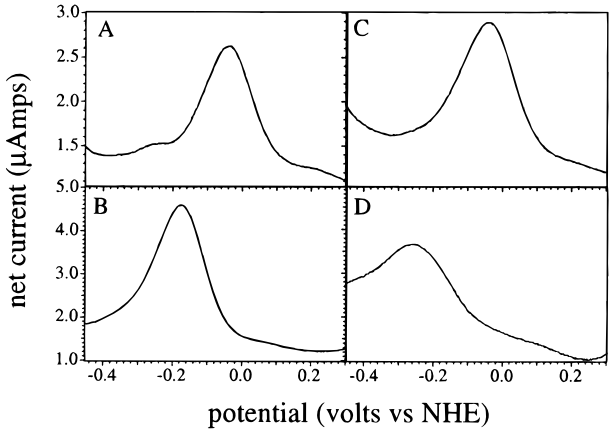

FIGURE 2: Square wave voltammograms of KatG and KatG(S315T) in the presence of isoniazid or cyanide. The applied potential waveform at a graphite electrode was $E_p = 25$ mV and $\tau^{-1} = 8$ Hz: (A) 200 μM KatG and 400 μM isoniazid, (B) 200 μM KatG and 200 μM sodium cyanide, (C) 200 μM KatG(S315T) and 400 μM isoniazid, and (D) 200 μM KatG(S315T) and 200 μM sodium cyanide.

Effect of Isoniazid and CN^- on KatG and KatG(S315T) Reduction Potentials. Addition of isoniazid to KatG or KatG(S315T) caused little, if any, change in the respective square wave voltammograms, each of which had peaks centered at ca. −40 mV versus the NHE (Figure 2A,C). Cyanide is known to bind as the sixth ligand of heme proteins, causing the heme to adopt a low-spin configuration. Addition of cyanide caused a decrease in the reduction potential of KatG, shifting the peak maximum to ca. −190 mV versus the NHE (Figure 2B). Addition of cyanide shifted the KatG(S315T) peak to ca. −250 mV (Figure 2D). The results of repeated experiments are summarized in Table 1.

Spectroelectrochemistry. Oxidative and reductive titrations were conducted for KatG and KatG(S315T), with the reductive titrations shown in Figure 3. Reduction of KatG (Figure 3A) caused a red shift of the heme Soret band to ∼430 nm, decreased Soret intensity, and increased the intensity of the α/β bands at 556 nm. The reaction was reversible as judged by restoration of the heme Soret band to its original wavelength and intensity following reoxidation by ferricyanide (data not shown). A plot of the normalized Soret absorbance as a function of potential for oxidized (A_{408}) and reduced (A_{430}) KatG is shown in the inset. Fitting the experimental data to the Nernst equation indicated a one-electron process with a reduction midpoint potential of −28 ± 17 mV versus the NHE (Table 1).

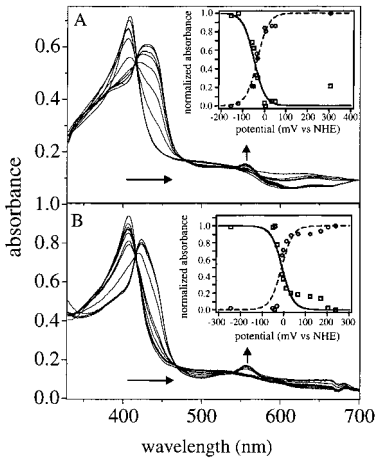

FIGURE 3: Spectroelectrochemical titrations of KatG and KatG(S315T). Solutions contained (A) 9 μM KatG or (B) 9 μM KatG(S315T) in 50 mM sodium phosphate buffer (pH 7.5) with the mediators described in Materials and Methods. The titrant was 50 mM sodium dithionite. Insets show the titration progress curves: (□) normalized absorbance at 408 nm (oxidized enzyme) and (○) normalized absorbance at 430 nm (reduced KatG) or 424 nm [reduced KatG(S315T)]. Lines represent the fit of the experimental data to the Nernst equation ($n = 1$). The normalized absorbance is defined as $(A_{408} - A_{408min})/(A_{408max} - A_{408min})$ (using the oxidized enzyme as an example).

Reduction of KatG(S315T) also caused a red shift of the Soret band (Figure 3B), although the band is sharper than that seen for wild-type KatG. As with KatG, the reaction was reversible as judged by restoration of the heme Soret band to its original wavelength and intensity following reoxidation by ferricyanide (data not shown). The Soret maximum for reduced KatG(S315T) was 424 nm, and increased intensity was also seen for the α/β bands at ~557 nm. The inset (Figure 3B) shows the absorbance of oxidized (A_{408}) and reduced (A_{424}) KatG(S315T) as a function of potential. Fitting to the Nernst equation indicated a one-electron process with a midpoint potential of -21 ± 18 mV versus the NHE (Table 1). The spectroelectrochemical titrations and square wave voltammograms for KatG and KatG(S315T) suggest another redox process may be occurring at ~200 mV (Figure 2B,D and Figure 3 insets) which we did not attempt to fit in the insets of Figure 3.

Isoniazid Reduction Potentials. The cyclic voltammograms for isoniazid (Figure 4A) suggest the drug undergoes three redox transitions between 0.8 and -0.8 V versus the NHE (designated by asterisks in Figure 4A). Again, the lack of a return wave makes it difficult to determine $E°$ from the cyclic voltammograms. Using the assumption described earlier, isoniazid was estimated to have reduction potentials at ca. -530, -260, and 470 mV versus the NHE.

The square wave voltammogram for isoniazid indicates reduction potentials at ca. -550, -190, and 500 mV versus the NHE. In SWV, a completely reversible reaction produces a symmetrical peak with a peak width at half-height of $126/n$, where n is the number of electrons transferred in the reaction (*29*). The isoniazid peaks in Figure 4B have widths at half-height between 134 and 200 mV and, assuming a one-electron process at each reduction potential, are wider than expected for a reversible reaction. Therefore, even at the rapid scan rates that are possible in SWV, it appears that an irreversible chemical reaction is responsible for the appearance of poorly defined peaks at each reduction potential.

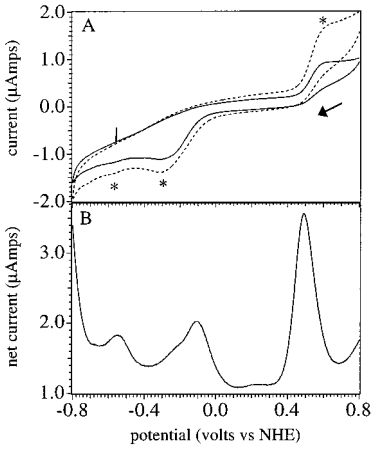

FIGURE 4: Voltammograms of isoniazid at a graphite electrode. The solution contained 200 μM isoniazid in 100 mM sodium phosphate buffer (pH 7.6) and 100 mM KCl: (A) cyclic voltammograms with sweep rates of 10 (solid line) and 20 mV/s (dashed line) and (B) square wave voltammogram with an applied potential waveform of $E_p = 25$ mV and $\tau^{-1} = 8$ Hz.

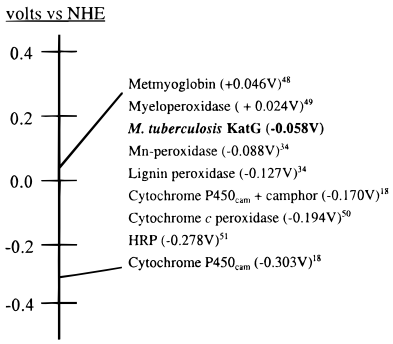

FIGURE 5: Redox potentials of selected heme proteins.

DISCUSSION

The square wave voltammograms of *M. tuberculosis* KatG indicate the heme iron undergoes reversible reduction to the ferrous state at ca. -58 mV versus the NHE. In addition, spectroelectrochemical titrations report a reduction potential of ca. -28 mV versus the NHE, so within the error of the measurements, two complementary techniques yield similar reduction potentials for wild-type KatG. The redox potential of KatG is in a range typical of hemoproteins (Figure 5) and is most similar to that of the Mn^{2+}-dependent peroxidase of *Phanerochaete chrysosporium* which contains a five-coordinate high-spin heme (*30*). However, the redox potential of KatG is approximately 200 mV higher than those of other peroxidases such as horseradish peroxidase (HRP), which is a mixture of five-coordinate and six-coordinate high-spin heme at room temperature (*31*). It has been suggested that the redox potential of hemoproteins is dependent on the nature and strength the sixth ligand to the iron as well as electrostatic, hydrophobic, and hydrogen bonding interactions within the heme cavity (*32*−*34*). The relatively high redox potential of KatG suggests that the sixth ligand to the heme is labile compared with that of HRP.

Binding of a strong ligand like cyanide causes a high- to low-spin transition of the heme iron. Cyanide binding at the heme iron of KatG and KatG(S315T) converts both to six-

coordinate low-spin heme (*20*). As expected, cyanide binding caused a decrease of ca. −150 to −200 mV in the reduction potentials of both enzymes, supporting the idea that a strong sixth ligand would make reduction of the heme iron more difficult. Comparison of the cyanide-bound and -free potentials of both enzymes also provides evidence consistent with a relatively weak sixth ligand for the resting ferric state of KatG and KatG(S315T). The strength of the sixth ligand to the heme is a measure of iron accessibility to exogenous oxidants such as H_2O_2 or superoxide.

Previous workers have shown that heme propionates can affect the heme redox potential by controlling the heme orientation or via a pH-dependent electrostatic interaction with the heme iron (*35*, *36*). Therefore, we thought it logical to examine the redox effects of mutating a critical residue like serine 315. Serine 315 has been hypothesized to form hydrogen bonds to the heme propionate, while the mutation to threonine has been shown to alter the electronic environment of the heme iron (*11*, *20*). Square wave voltammetry and spectroelectrochemical titrations indicate that the redox potential of KatG(S315T) is essentially identical to that of wild-type KatG (Table 1). The S315T mutation therefore does not confer isoniazid resistance due to a change in the reduction potential of the heme Fe^{3+}/Fe^{2+} couple.

Substrate binding by cytochrome P450 oxygenases is often associated with an increase in the reduction potential of the heme iron. For example, binding of the substrate camphor by cytochrome $P450_{cam}$ causes a 123 mV increase in its redox potential (*37*). Since it has been suggested that KatG may oxidize isoniazid using a P450-like mechanism (*7*), we examined the effect of isoniazid on the midpoint potential of KatG and isoniazid-resistant KatG(S315T). Isoniazid binding had little effect on the redox potential of either KatG (Figure 2A) or KatG(S315T) (Figure 2C) and therefore does not cause changes typical of P450-like enzymes. It is still possible, however, that KatG utilizes a P450-like mechanism but does not require a significant redox shift prior to oxygen activation of the heme iron due to the relatively high heme midpoint potential. Precedence is provided by rat liver microsomal cytochrome P450 which does not undergo a redox potential shift prior to substrate oxidation (*38*, *39*).

Square wave and cyclic voltammograms of isoniazid indicate the antibiotic is oxidized at ∼0.5 V versus the NHE. This value is in good agreement with those of Hansen et al., who reported a potential centered at ∼0.5 V versus the NHE using differential pulse polarography, and Tong et al., who reported an anodic current with a maximum at ∼0.5 V versus the NHE using cyclic voltammetry, although the latter group saw an oxidation wave only in the presence of the 2,2,6,6-tetramethyl-4-acetylpiperidine-1-oxy radical (*40*, *41*). Consistent with our findings, the voltammogram was irreversible, failing to exhibit a return cathodic wave. We suggest that this potential corresponds to a one-electron oxidation of isoniazid's hydrazine moiety to a hydrazyl radical:

$$RCONHNH_2 \rightarrow RCONHNH^{\bullet} + 1e^- + H^+ \ (R = \text{pyridine}) \quad (2)$$

Isoniazid also appears to undergo two distinct reduction steps centered at ca. −0.2 and −0.6 V versus the NHE. Neuss et al., using polarography at a dropping mercury electrode, reported that isoniazid exhibits two reduction waves centered at ca. −0.4 and −0.5 V versus the NHE at pH <1.5, which coalesced into a single wave as the pH was raised above 1.5 (*42*).

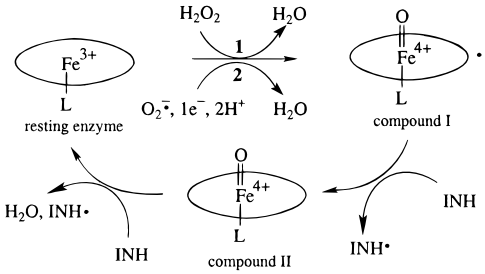

FIGURE 6: Proposed mechanism for the KatG-mediated one-electron oxidation of isoniazid to a hydrazyl radical. Compound I can be formed by (1) the peroxidase pathway of KatG using a peroxide as the extraneous oxidant or (2) the oxyferrous pathway using superoxide as the oxidant. L represents the endogenous fifth heme ligand of KatG. INH represents isoniazid, and INH• represents the hydrazyl radical of isoniazid.

The results indicate that, in its resting ferric state, the redox potential of wild-type KatG ($E° \approx -0.06$ V) is not sufficient to oxidize isoniazid ($E° \approx 0.5$ V) without further activation of the heme iron to a high-valent intermediate like compounds I and II or oxyferrous KatG. Indeed, a requirement for an extraneous oxidant such as dioxygen or a peroxide has been reported both in vitro (*7*, *17*, *43*) and in vivo (*44*, *45*). The redox potentials of compounds I and II of HRP have been reported to be ∼0.9 V versus the NHE while the potential of the formal cytochrome P450 (Fe^{3+}═O) species (analogous to peroxidase compound I) is estimated to be 1.5−2.0 V (*46*, *47*). Although not yet reported, it seems reasonable to suggest that KatG compounds I and II or oxyferrous KatG will have similarly high potentials which would be sufficient to initiate isoniazid oxidation. A proposed mechanism for the one-electron oxidation of isoniazid to a hydrazyl radical by a high-valent KatG intermediate is presented in Figure 6. The fate of the hydrazyl radical is not known, but we postulate that it may dimerize or can be further oxidized to isonicotinic acid, isonicotinamide, and pyridine-4-carboxyaldehyde which are the known, stable products of isoniazid oxidation by KatG (*2*).

In summary, the reduction potential of KatG was determined to be ca. −58 mV versus the NHE using square wave voltammetry and spectroelectrochemical titrations. Neither the clinically important S315T mutation nor binding of isoniazid affected the reduction potential, suggesting the ability to convert the KatG iron from the ferric to ferrous oxidation state is not altered in isoniazid-resistant strains of *M. tuberculosis* harboring KatG(S315T). The results also provide evidence for the paradigm that isoniazid oxidation by KatG proceeds by a mechanism requiring the formation of higher-potential intermediates such as compound I, compound II, or oxyferrous KatG.

REFERENCES

1. World Health Organization (1999) *World Health Report*, Geneva
2. Johnsson, K., and Schultz, P. G. (1994) *J. Am. Chem. Soc. 116*, 7425−7426.
3. Marcinkeviciene, J. A., Magliozzo, R. S., and Blanchard, J. S. (1995) *J. Biol. Chem. 270*, 22290−22295.
4. Johnsson, K., Froland, W. A., and Schultz, P. G. (1997) *J. Biol. Chem. 272*, 2834−2840.

5. Magliozzo, R. S., and Marcinkeviciene, J. A. (1997) *J. Biol. Chem. 272*, 8867−8870.
6. Wengenack, N. L., Uhl, J. R., St. Amand, A. L., Tomlinson, A. J., Benson, L. M., Naylor, S., Kline, B. C., Cockerill, F. R., and Rusnak, F. (1997) *J. Infect. Dis. 176*, 722−727.
7. Magliozzo, R. S., and Marcinkeviciene, J. A. (1996) *J. Am. Chem. Soc. 118*, 11303−11304.
8. Wengenack, N. L., Jensen, M. P., Rusnak, F., and Stern, M. K. (1999) *Biochem. Biophys. Res. Commun. 256*, 485−487.
9. Rozwarski, D. A., Grant, G. A., Barton, D. H. R., Jacobs, W. R., Jr., and Sacchettini, J. C. (1998) *Science 279*, 98−102.
10. Mdluli, K., Slayden, R. A., Zhu, Y., Ramaswamy, S., Pan, X., Mead, D., Crane, D. D., Musser, J. M., and Barry, C. E., III (1998) *Science 280*, 1607−1610.
11. Heym, B., Alzari, P. M., Honore, N., and Cole, S. T. (1995) *Mol. Microbiol. 15*, 235−245.
12. Musser, J. M., Kapur, V., Williams, D. L., Kreiswirth, B. N., van Soolingen, D., and van Embden, J. D. A. (1996) *J. Infect. Dis. 173*, 196−202.
13. Ramaswamy, S., and Musser, J. M. (1998) *Tuberc. Lung Dis. 79*, 3−29.
14. Victor, T. C., Pretorius, G. S., Felix, J. V., Jordaan, A. M., van Helden, P. D., and Eisenach, K. D. (1996) *Antimicrob. Agents Chemother. 40*, 1572.
15. Rouse, D. A., DeVito, J. A., Li, Z., Byer, H., and Morris, S. L. (1996) *Mol. Microbiol. 22*, 583−592.
16. Uhl, J. R., Sandhu, G. S., Kline, B. C., and Cockerill, F. R., III (1996) in *PCR Protocols for Emerging Infectious Diseases* (Persing, D., Ed.) pp 144−149, ASM Press, Washington, DC.
17. Wengenack, N. L., Hoard, H. M., and Rusnak, F. (1999) *J. Am. Chem. Soc. 121*, 9748−9749.
18. Sligar, S. G., Cinti, D. L., Gibson, G. G., and Schenkman, J. B. (1979) *Biochem. Biophys. Res. Commun. 90*, 925−932.
19. Sono, M., Roach, M. P., Coulter, E. D., and Dawson, J. H. (1996) *Chem. Rev. 96*, 2841−2887.
20. Wengenack, N. L., Todorovic, S., Yu, L., and Rusnak, F. (1998) *Biochemistry 37*, 15825−15834.
21. Saint-Joanis, B., Souchon, H., Wilming, M., Johnsson, K., Alzari, P. M., and Cole, S. T. (1999) *Biochem. J. 338*, 753−760.
22. Bradford, M. M. (1976) *Anal. Biochem. 72*, 248−254.
23. Maehly, A. C. (1955) *Methods Enzymol. 2*, 801−813.
24. Kissinger, P. T., and Heineman, W. R. (1983) *J. Chem. Educ. 60*, 702−706.
25. Osteryoung, J. (1988) *Methods Enzymol. 158*, 243−267.
26. Stankovich, M. T. (1980) *Anal. Biochem. 109*, 295−308.
27. Sawyer, D. T., and Roberts, J. L., Jr. (1974) in *Experimental Electrochemistry for Chemists*, John Wiley & Sons, New York.
28. Mabbott, G. A. (1983) *J. Chem. Educ. 60*, 697−701.
29. Smith, E. T., and Feinberg, B. A. (1990) *J. Biol. Chem. 265*, 14371−14376.
30. Millis, C. D., Cai, D., Stankovich, M. T., and Tien, M. (1989) *Biochemistry 28*, 8484−8489.
31. Evangelista-Kirkup, R., Crisanti, M., Poulos, T., and Spiro, T. G. (1985) *FEBS Lett. 190*, 221−226.
32. Moore, G. R., Pettigrew, G. W., and Rogers, N. K. (1986) *Proc. Natl. Acad. Sci. U.S.A. 83*, 4998−4999.
33. Kassner, R. J. (1972) *Proc. Natl. Acad. Sci. U.S.A. 69*, 2263−2267.
34. Mauk, A. G., and Moore, G. R. (1997) *J. Biol. Inorg. Chem. 2*, 119−125.
35. Das, D. K., and Medhi, O. K. (1998) *J. Inorg. Biochem. 70*, 83−90.
36. Adak, S., and Banerjee, R. (1998) *Biochem. J. 334*, 51−56.
37. Fisher, M. T., and Sligar, S. G. (1985) *J. Am. Chem. Soc. 107*, 5018−5019.
38. Guengerich, F. P., Ballou, D. P., and Coon, M. J. (1975) *J. Biol. Chem. 250*, 7405−7414.
39. Guengerich, F. P. (1983) *Biochemistry 22*, 2811−2820.
40. Hansen, E. B., Jr., Dooley, K. L., and Thompson, H. C., Jr. (1995) *J. Chromatogr. 670*, 259−266.
41. Tong, J., Dang, X., and Li, H. (1997) *Electroanalysis 9*, 165−168.
42. Neuss, J. D., Seagers, W. J., and Mader, W. J. (1952) *J. Am. Pharm. Assoc. 41*, 670−673.
43. Zabinski, R. F., and Blanchard, J. S. (1997) *J. Am. Chem. Soc. 119*, 2331−2332.
44. Youatt, J. (1969) *Am. Rev. Respir. Dis. 99*, 729−749.
45. Takayama, K., and Davidson, L. A. (1979) *Antibiotics 5*, 98−119.
46. Hayashi, Y., and Yamazaki, I. (1979) *J. Biol. Chem. 254*, 9101−9106.
47. Guengerich, F. P., and Macdonald, T. L. (1984) *Acc. Chem. Res. 17*, 9−16.
48. Taylor, J. F., and Morgan, V. E. (1942) *J. Biol. Chem. 144*, 15−20.
49. Ikeda-Saito, M., and Prince, R. C. (1985) *J. Biol. Chem. 260*, 8301−8305.
50. Conroy, C. W., Tyma, P., Daum, P. H., and Erman, J. E. (1978) *Biochim. Biophys. Acta 537*, 62−69.
51. Makino, R., Chiang, R., and Hager, L. P. (1976) *Biochemistry 15*, 4748−4754.

BI001239V